# Gas-Transport and Thermal Properties of a Microphase-Ordered Poly(styrene-*b*-ethylene oxide-*b*-styrene) Triblock Copolymer and Its Blends with Poly(ethylene glycol)

**Nikunj P. Patel[†] and Richard J. Spontak*[,†,‡]**

*Departments of Chemical Engineering and Materials Science & Engineering, North Carolina State University, Raleigh, North Carolina 27695*

*Received January 2, 2004; Revised Manuscript Received January 30, 2004*

ABSTRACT: Block copolymers are under growing consideration as precursor materials for use in a wide variety of emerging nanotechnologies. While these materials can serve as ordered templates in the preparation of nanoporous membranes, they can also be designed for use as dense nanostructured polymer membranes exhibiting chemical specificity. In the present work, we explore the properties of a poly(styrene-*b*-ethylene oxide-*b*-styrene) (SEOS) triblock copolymer and its blends with poly(ethylene glycol) (PEG) as reverse-selective membranes due to their unusually high $CO_2$ affinity. The permeability of $CO_2$ measured as a function of blend composition, PEG molecular weight, and temperature is consistently found to exceed that of any other gas ($H_2$, $N_2$, or $O_2$) examined here. Addition of PEG eventually results in a composition-dependent transition from an alternating lamellar to polyether-continuous morphology, as evidenced by both gas-transport and thermal properties, and a systematic variation in crystallinity that depends on PEG molecular weight. Since the microphase-ordered copolymer morphology remains intact up to temperatures higher than the polyether melting temperature, the changes in permeability that occur upon polyether melting can be directly measured.

## Introduction

Because of their highly ordered nanostructures[1−3] and the development of design paradigms[4] to generate nanostructures of particular size and shape, block copolymers and their miscible blends with solvents,[5,6] homopolymers,[7,8] and other copolymers[9−12] have become a central component of numerous nanotechnologies, including ultraporous membranes, waveguides, and capacitors.[13] Such applications often rely on using ordered block copolymers as templates to which *inorganic* species (e.g., nanoparticles[14] or ceramic precursors[15]) are added. One commercially relevant application of block copolymers and their blends with *organic* additives that has not received much attention is their use in selective gas separations.[16] Polymeric membranes constitute an attractive alternative to conventional separation processes (e.g., cryogenic distillation, absorption, and pressure-swing adsorption) in terms of low production cost as well as economical and reliable operation. While industrial membranes tend to separate gases on the basis of molecular size, allowing smaller molecules to concentrate on the permeate side,[17] the selective removal of acid gases such as $CO_2$ from mixed gases requires larger penetrant molecules to be more permeable than small ones for efficient and competitive membrane function.[18] Such "reverse-selective" membranes may be derived from (i) glassy polymers whose free volume is enhanced through the incorporation of nanoparticles[19] or (ii) rubbery polymers possessing polar moieties capable of interacting with acid gases. In the case of poly(ethylene glycol) (PEG), which exhibits high $CO_2$ solubility in its liquid form,[20] the intrinsic mechanical properties are unacceptably low for gas membrane applications but can be improved substantially via chemical cross-linking.[21,22]

A viable alternative to chemically cross-linking PEG (and introducing covalent linkages to generate a load-bearing network) is to incorporate PEG into a block copolymer that can, upon microphase separation, form a physically cross-linked nanostructure capable of exhibiting satisfactory mechanical properties. This requirement is readily met when low-molecular-weight PEG is copolymerized with a hard block that is either glassy or semicrystalline at application conditions. Indeed, this is the very strategy behind the development of $CO_2$-selective membranes derived from various polyether segmented copolymers wherein the hard block is either a polyamide or polyimide,[23−25] and the copolymers can best be described as randomly coupled, in contrast to perfectly alternating,[26] multiblock copolymers. These materials have been found to exhibit exceptional polar/nonpolar ($CO_2/H_2$ or $CO_2/N_2$) gas selectivity. Okamoto et al.[23] report that the $CO_2$ permeability ($P_{CO_2}$) in poly(ether-*b*-imide) segmented copolymers can be as high as 140 Barrers [1 Barrer = $10^{-10}$ $cm^3$ (STP) cm/($cm^2$ s cmHg)] with a corresponding $CO_2/N_2$ selectivity ($\alpha_{CO_2/N_2}$), defined as $P_{CO_2}/P_{N_2}$, of up to 70 at 25 °C. On the basis of these findings, they propose that such high $CO_2$ permeability and selectivity reflect an attractive interaction between $CO_2$ molecules, each with its quadrupolar moment, and the polar ether linkages in the PEG sequences. Bondar et al.[24] attribute similar behavior in a limited series of commercial poly(ether-*b*-amide) segmented copolymer to high $CO_2/H_2$ solubility selectivity, whereas Kim et al.[25] have observed that the permeability of nonpolar gases *decreases* with increasing penetrant size but that of polar gases *increases* with increasing penetrant size, in the same copolymer series.

Although segmented copolymers can, depending on their interblock incompatibility, microphase-separate into a load-bearing nanostructure, they tend not to microphase-order into periodic morphologies due to their high degree of block connectivity and the corresponding propensity for kinetic entrapment of the chains during

[†] Department of Chemical Engineering.
[‡] Department of Materials Science & Engineering.
* To whom correspondence should be addressed. E-mail Rich_Spontak@ncsu.edu.

10.1021/ma049975k CCC: $27.50 
Published on Web 03/24/2004

self-organization. The pioneering studies by Kinning et al.[27] and Cohen and co-workers[28] of nonselective gas transport through model microphase-ordered block copolymers derived from polystyrene (S) and a polydiene confirm that the extent of microphase separation, connectivity, and orientation relative to the diffusion axis, collectively expressed here as copolymer morphology, play a critical role in penetrant mobility.[29] Theoretical frameworks developed[28,30−32] to describe molecular transport through microphase-ordered block copolymers must likewise consider the features of the existing morphology. While most studies of gas transport through microphase-ordered block copolymers have focused on the conventional copolymers alluded to above, recent efforts by Arnold et al.[33] have sought to employ designer diblock/triblock copolymers for the selective permeation of particular penetrants. It is in this spirit that this work examines the permeation of polar and nonpolar gases through a microphase-ordered triblock copolymer with a polyether midblock. Miscible blends of this copolymer with PEG are used to ascertain the effect of blend composition and, hence, morphology on these properties as well as on accompanying thermal characteristics. Because the copolymer end blocks remain glassy over the range of temperatures explored here, the neat copolymer and its blends with PEG behave as physically cross-linked networks, thereby allowing investigation of gas-transport properties above and below the melting point of the polyether.

## Experimental Section

**Materials.** A poly(styrene-*b*-ethylene oxide-*b*-styrene) (SEOS) triblock copolymer was obtained from Polymer Source, Inc. (Dorval, Canada). According to $^1$H NMR and GPC analyses conducted by the manufacturer, the composition, number-average molecular weight, and polydispersity of the copolymer were 43 wt % EO, 69 000, and 1.03, respectively. Two PEG oligomers with molecular weights of 400 ($PEG_{400}$, a liquid at 25 °C) and 4600 ($PEG_{4600}$, a semicrystalline powder at 25 °C) were purchased from Aldrich (Milwaukee, WI) and used as received. Solvent-grade chloroform was likewise purchased from Aldrich and used without further purification.

**Methods.** Bulk films of the copolymer with and without PEG were prepared by dissolving predetermined quantities of the constituent species in chloroform at a polymer concentration of 5−10% w/v. Each solution was stirred at ambient temperature until it became visibly clear and then cast into Teflon molds wherein the solvent was permitted to evaporate over a period of 3−4 days at ambient temperature. The resultant films appeared macroscopically defect-free and were subjected to annealing at 95 °C for 24 h to remove residual solvent and promote nanostructural refinement. Following annealing, each film, ranging from 80 to 160 $\mu$m in thickness, was sandwiched between Al foil so that a circular area of 0.785 cm$^2$ was available for gas permeation. Pure-gas permeation properties of the neat SEOS copolymer and its blends were measured by the constant-volume/variable-pressure method described elsewhere.[34] The setup used here consisted of a downstream vessel of known volume ($V$), a permeation cell containing a polymer film, and an upstream vessel maintained at a designated temperature. Vacuum was pulled on both sides of the film before exposing the upstream side to a desired gas pressure ($p_2$). As the gas permeated through the film, the pressure on the downstream side was monitored until the pressure increase rate ($dp/dt$) remained constant. The permeability of the gas was determined from

$$P_i = (Vl/ARTp_2)(dp/dt) \tag{1}$$

where $l$ is the film thickness, $A$ is the exposed film area, $R$ is the gas constant, and $T$ denotes absolute temperature. In all the permeation tests discussed here, the highest downstream pressure was 0.007 atm, in which case $p_2$ effectively corresponds to the transmembrane pressure. All permeation tests were conducted at 35 °C unless otherwise specified.

The thermal characteristics of the SEOS copolymer, SEOS/PEG blends, and the $PEG_{4600}$ homopolymer were measured by differential scanning calorimetry (DSC) with a Perkin-Elmer DSC-7 unit calibrated with respect to In. Data were collected under a nitrogen blanket in a heat−cool−reheat cycle wherein the specimens were heated to 200 °C, cooled to −50 °C, and then reheated to 200 °C. The heating rate in the reheat cycle was held constant at 20 °C/min. The normal melting temperatures reported herein correspond to peak temperatures observed during the reheat cycle, and the corresponding percent crystallinity ($X_c$) is calculated from

$$X_c = 100\% \times \Delta H_m/(W_{EO}\Delta H_m°) \tag{2}$$

where $\Delta H_m$ is the latent heat of melting approximated by the area under the melting endotherm and $\Delta H_m°$ is the latent heat of melting for 100% crystalline poly(ethylene oxide) (186.188 J/g, as reported elsewhere[35]). The composition $W_{EO}$ denotes the weight fraction of crystallizable polyether and is given by $w_{EO}(1 - w_{PEG}/100) + w_{PEG}/100$, where $w_{EO}$ is the weight fraction of the EO block in the copolymer (0.43) and $w_{PEG}$ is the weight percentage of added PEG. Optical micrographs of the neat copolymer and several blends were acquired under crossed polars at 25 °C with an Olympus BX60 microscope. Images were collected digitally with a CCD camera.

## Results and Discussion

**Factors Governing Gas Transport.** The permeability of penetrant $i$ ($P_i$) through a dense polymer film is generally given by

$$P_i = N_i l/\Delta p_i \tag{3}$$

where $N_i$ is the steady-state gas flux of species $i$ through the film, and $\Delta p_i = p_{2i} - p_{1i}$, with $p_{2i}$ and $p_{1i}$ being the upstream and downstream partial pressures of $i$, respectively. When $p_{1i}$ is negligible relative to $p_{2i}$ and Fickian diffusion constitutes the rate-limiting step in penetrant transport, the permeability can be conveniently written in terms of the solution−diffusion model for nonporous (dense) polymer membranes[36] as

$$P_i = D_i S_i \tag{4}$$

Here, $D_i$ is the concentration-averaged effective diffusion coefficient, and $S_i$ is the solubility defined as the ratio of penetrant concentration dissolved in the upstream face relative to the upstream partial pressure in the gas phase. According to the solution−diffusion model, penetrant molecules dissolve into the upstream (high pressure) face of the film, diffuse across the film, and ultimately desorb at the downstream (low pressure) face. Thus, depending on their diffusivity and solubility within a given polymer, different penetrants exhibit different permeabilities. The permeability of penetrant A relative to that of penetrant B is commonly expressed by the ideal selectivity ($\alpha_{A/B}$), which is defined as

$$\alpha_{A/B} = P_A/P_B = (D_A/D_B)(S_A/S_B) \tag{5}$$

The ratio $D_A/D_B$ is termed the diffusivity, or mobility, selectivity, whereas $S_A/S_B$ is known as the solubility selectivity.[37] Gas solubility is sensitive to factors such as operating conditions, penetrant condensability, polymer−penetrant interaction, and polymer morphology (crystallinity and molecular orientation). The diffusion

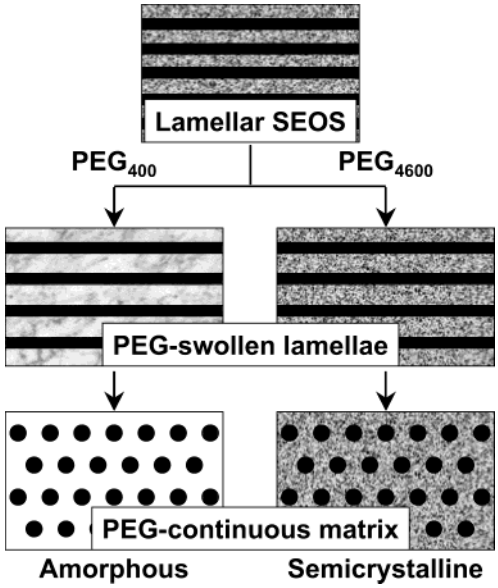


**Figure 1.** Schematic illustration of the blending strategy proposed here to probe the effects of blend composition (morphology) and crystallinity on the gas-permeation properties of a microphase-ordered SEOS triblock copolymer that exhibits the lamellar morphology. Addition of either $PEG_{400}$ (amorphous) or $PEG_{4600}$ (semicrystalline) initially swells, as well as alters the crystallinity of, the host EO lamellae. Further addition of either PEG is anticipated to promote an order−order transition to a polyether-continuous morphology wherein the PEG-rich matrix is either principally amorphous ($PEG_{400}$) or semicrystalline ($PEG_{4600}$).

coefficient also depends on penetrant size, polymer morphology, and polymer segmental dynamics.[38]

With these considerations in mind, we now turn our attention to the strategy adopted here for controllably altering the composition and, hence, morphology and, ultimately, the gas-transport properties of a microphase-ordered SEOS copolymer (illustrated in Figure 1). The neat copolymer exhibits a lamellar morphology, as evidenced by its composition and transmission electron microscopy (TEM) images.[39] While the S microphases (colored black in Figure 1) are glassy at ambient temperature, the EO microphases (speckled in the top of Figure 1) are semicrystalline due to the relatively high molecular weight of the copolymer midblock (∼30 000). Addition of $PEG_{4600}$, a semicrystalline homopolymer, to the SEOS copolymer should promote lamellar swelling and, eventually, a transition to a polyether-continuous morphology wherein the polyether microphase remains semicrystalline, which is unfavorable for molecular transport. If, on the other hand, $PEG_{400}$, an amorphous liquid at ambient temperature, is used in analogous fashion, the degree of midblock crystallinity is expected to decrease with increasing $PEG_{400}$ concentration. A reduction in polyether crystallinity will improve penetrant solubility, which is crucial to the design of $CO_2$-selective membranes, and diffusivity (through the removal of obstacles impeding molecular mobility). Thus, by judicious selection of blend composition and PEG homopolymer, an amorphous, polyether-continuous morphology with improved $CO_2$ permeability and selectivity relative to nonpolar gases should be achievable through physical modification of the semicrystalline SEOS copolymer. The viability of this strategy is supported by results recently obtained[40] by sorbing PEG of different molecular weights from selective solvents (e.g., water and ethanol) into the same

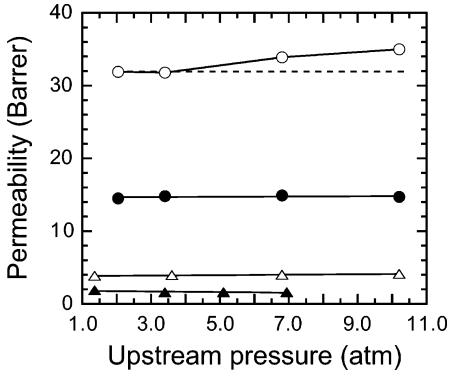


**Figure 2.** Dependence of permeability on upstream (transmembrane) pressure for four gases—$CO_2$ (○), $H_2$ (●), $O_2$ (△), and $N_2$ (▲)—through the neat SEOS triblock copolymer at 35 °C. The solid lines connect the data, whereas the dashed line corresponds to constant permeability for $CO_2$.

microphase-ordered SEOS copolymer, as well as into the poly(ether-*b*-amide) multiblock copolymer discussed earlier, to form "mesoblends".

**Gas Transport in SEOS/PEG Blends.** The permeability data presented as a function of upstream (or, equivalently, transmembrane) pressure in Figure 2 for the neat SEOS copolymer indicate that the copolymer, despite its intrinsic crystallinity, behaves as a $CO_2$-selective membrane. Over the entire pressure range examined at ambient temperature, the permeability of $CO_2$ is clearly the highest of all the gases investigated, followed by $H_2$, $O_2$, and then $N_2$. Since this order is comparable to that observed with regard to rubbery polymers such as poly(dimethylsiloxane)[41] and *cis*-polyisoprene,[42] permeation through the SEOS copolymer is expected to occur primarily through the amorphous (rubbery) region of the EO lamellae. Another feature of the data shown in Figure 2 is that only the $CO_2$ permeability appears to be pressure-dependent. This characteristic behavior has likewise been observed in polyether-containing segmented copolymers[24] and cross-linked PEG.[22] Selectivity ranges based on eq 5 and extracted from the data in Figure 2 are as follows: 2.1−2.4 for $CO_2/H_2$, 8.1−8.5 for $CO_2/O_2$, and 17−22 for $CO_2/N_2$. While these selectivity ranges are low relative to, for instance, those measured from chemically cross-linked PEG diacrylate with a molecular weight of 700 (9.5−11 for $CO_2/H_2$, 26−30 for $CO_2/O_2$, and 68 to 84 for $CO_2/N_2$),[22] Figure 2 confirms that the presence of a polyether block within the copolymer promotes $CO_2$ specificity. The apparent reduction in chemical specificity compared to pure (cross-linked) PEG can be attributed to a combination of (i) the crystallinity of the polyether midblock and (ii) the nonspecificity of the S microdomains. Systematic variation of polyether crystallinity through physical incorporation of PEG is the topic of further discussion in subsequent sections. The permeability of each gas used in Figure 2 through homopolystyrene can be determined from its temperature dependence since Arrhenius behavior is observed.[43] In this case the permeability is given by

$$P = P_0 \exp(-E_P/RT) \tag{6}$$

where $P_0$ is the frequency factor and $E_P$ is the apparent activation energy for permeation. Values of $P_0$ and $E_P$ reported by Yamada and Nakagawa[43] are listed in Table 1 and yield the following permeabilities at 35 °C (in Barrers): 14 for $CO_2$, 27 for $H_2$, 2.9 for $O_2$, and 0.51 for

**Table 1. Frequency Factors and Apparent Activation Energies for Several Gases in Glassy Polystyrene[a]**

| gas | $P_0$ ($10^3$ Barrers) | $E_P$ (kJ/mol) |
|---|---|---|
| $H_2$ | 9.67 | 15.1 |
| $N_2$ | 6.99 | 24.4 |
| $O_2$ | 2.91 | 17.7 |
| $CO_2$ | 0.38 | 8.41 |

[a] Data from Yamada and Nakagawa.[43]

$N_2$. For completeness, the corresponding $CO_2/H_2$, $CO_2/O_2$, and $CO_2/N_2$ selectivities are calculated to be 0.54, 4.9, and 28, respectively, confirming that the $CO_2/H_2$ selectivity of this SEOS triblock copolymer membrane is regrettably compromised by the presence of $H_2$-selective S microdomains.

The permeation results displayed in Figure 2 can also be used as a probe of the copolymer morphology. Since both microphases of the copolymer are permeable to the gases investigated here, we employ the permeability relationships proposed by Robeson et al.[44] as extensions to the model originally developed by Maxwell[45] to describe the dielectric properties of a suspension of solid spheres. For a lamellar morphology in which the lamellae lie normal to the direction of flow (the series orientation), the net permeability can be expressed as

$$P = P_S P_{EO}/(\phi_S P_{EO} + \phi_{EO,a} P_S) \quad (7a)$$

where $\phi_i$ ($i$ = S or EO) is the volume fraction of $i$, and the designation "a" signifies the amorphous fraction. In the parallel orientation with the lamellae lying along the direction of penetrant flow, the net permeability is written as

$$P = \phi_S P_S + \phi_{EO,a} P_{EO} \quad (7b)$$

While the block copolymer possesses a lamellar morphology in which the lamellae are oriented within a single grain, grains will exhibit different orientations with respect to the direction of penetrant flow. Thus, the copolymer can be considered microscopically anisotropic but macroscopically isotropic,[28] in which case eqs 7a and 7b are used to determine the permeability limits corresponding to each orientation. Alternative approaches such as those discussed by Subramanian and Plotzker[46] could likewise be applied to discern, for example, the crystallinity of the neat copolymer, but thermal calorimetry can be used with greater accuracy for this purpose.

The permeabilities of $CO_2$, $H_2$, $O_2$, and $N_2$ in the SEOS triblock copolymer and a low-density polyethylene,[47] which resembles PEG in terms of chemical structure, are presented as a function of penetrant normal boiling point ($T_b$), an established[48] measure of condensability (solubility), in Figure 3a. In both cases, $CO_2$ is observed to be more permeable than any of the other gases investigated. The corresponding selectivity of each gas relative to $H_2$ is included in Figure 3b and reveals that the $N_2/H_2$ and $O_2/H_2$ selectivities are virtually identical for the SEOS copolymer and the polyethylene. Once again, however, the $CO_2/H_2$ selectivity is noticeably higher in the copolymer. This apparent trend can be explained in terms of the physical properties[49,50] of $CO_2$ and $H_2$, which are provided in Table 2. While the normal boiling point (or critical temperature) can be considered a good measure of gas solubility, the critical volume is a indicator of penetrant diffusivity.[37] Since $H_2$ is smaller than $CO_2$, $H_2$ possesses a higher diffusion coefficient

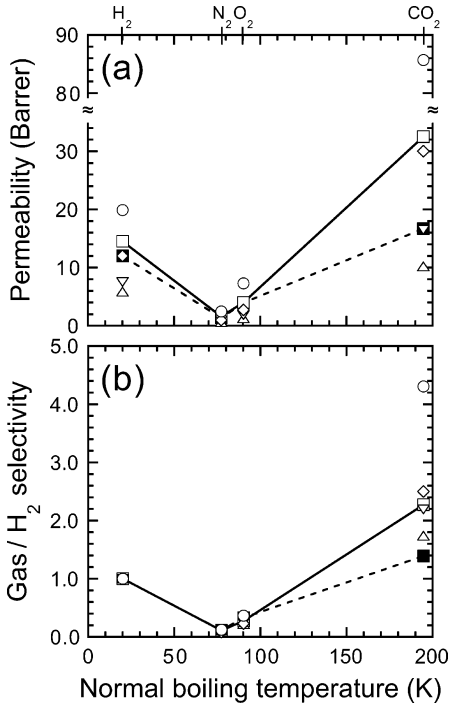


**Figure 3.** Variation of (a) permeability and (b) selectivity relative to $H_2$ with normal boiling temperature, a measure of gas condensability within a dense polymer membrane, for the neat SEOS copolymer (□, connected by a solid line) and four SEOS/PEG blends: 20 wt % $PEG_{4600}$ (△), 45 wt % $PEG_{4600}$ (▽), 22 wt % $PEG_{400}$ (◇), and 45 wt % $PEG_{400}$ (○). Results obtained for a low-density polyethylene (■, connected by a dashed line) are included for comparison.

**Table 2. Pertinent Physical Characteristics of $CO_2$ and $H_2$**

| | penetrant size | | condensability | |
|---|---|---|---|---|
| gas | critical vol[a] ($cm^3$/mol) | kinetic diam[b] (nm) | normal boiling point[a] (K) | critical temp[b] (K) |
| $H_2$ | 65.1 | 0.29 | 20.4 | 33.2 |
| $CO_2$ | 93.9 | 0.33 | 194.7 | 304.1 |

[a] Data from Reid et al.[49] [b] Data from Breck.[50]

than $CO_2$, in which case $D_{CO_2}/D_{H_2} < 1$. Conversely, $CO_2$ is more soluble than $H_2$ due to its higher condensability. This thermodynamic aspect, coupled with specific interactions between $CO_2$ molecules and the polar linkages of amorphous PEG, increases the $CO_2/H_2$ solubility selectivity sufficiently to not only overcome the effect of reduced $CO_2/H_2$ mobility selectivity (see eq 5) but also yield an overall $CO_2/H_2$ selectivity that is markedly greater than unity (~2.3). Thus, it immediately follows that, due to its enhanced solubility in the amorphous regions of the EO lamellae, $CO_2$ is more permeable in the SEOS copolymer membrane than $H_2$.

Addition of $PEG_{4600}$ to the SEOS copolymer at concentrations of 20 and 45 wt % yields the results included in Figure 3. At both $PEG_{4600}$ concentrations, the permeability of each gas decreases (see Figure 3a), as does the $CO_2/H_2$ selectivity (see Figure 3b). If $PEG_{400}$ is added at a concentration of 22 wt %, neither the $CO_2$ permeability nor the $CO_2/H_2$ selectivity changes significantly from that of the neat copolymer. At a concentration of 45 wt % $PEG_{400}$, however, $P_{CO_2}$ increases markedly (from ~33 for the neat copolymer to ~86 in the blend) in conjunction with a substantial increase in $\alpha_{CO_2/H_2}$ (from 2.3 to 4.3). To put this increase in perspective, the $CO_2/H_2$ selectivity of poly(dimethylsiloxane) is re-

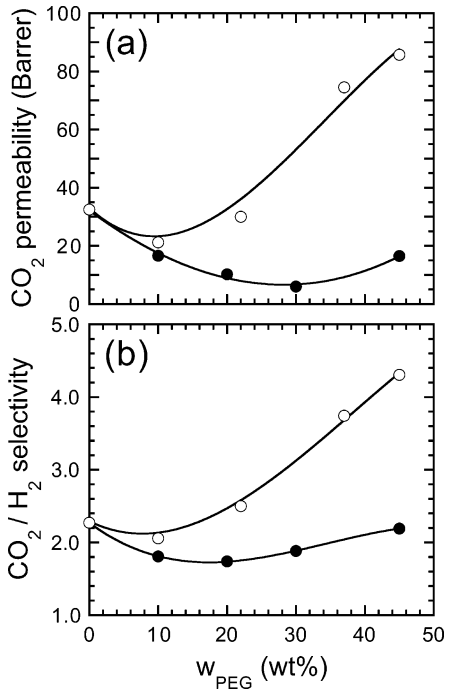


**Figure 4.** Dependence of (a) $CO_2$ permeability and (b) $CO_2/H_2$ selectivity on blend composition in SEOS/PEG blends containing $PEG_{400}$ (○) and $PEG_{4600}$ (●). The solid lines serve as guides for the eye.

ported[41] to be ~3.6 at 35 °C. The effects of PEG concentration and molecular weight on $CO_2$ permeability and $CO_2/H_2$ selectivity are shown for two series of SEOS/PEG blends in Figure 4. For blends prepared with either $PEG_{400}$ or $PEG_{4600}$, an upper limit of ca. 45 wt % PEG is dictated by the mechanical stability of the films used in the permeation analysis. As first observed in Figure 3, addition of $PEG_{4600}$ to the SEOS copolymer promotes a general reduction in $P_{CO_2}$ (Figure 4a), as well as a decrease in $CO_2/H_2$ selectivity, over most of the blend composition range explored (Figure 4b). Only at high $PEG_{4600}$ concentrations (>45 wt %) is a $CO_2/H_2$ selectivity comparable to that of the neat copolymer recovered. If $PEG_{400}$ is added to the copolymer, very different results are obtained. At $PEG_{400}$ concentrations typically less than ~20 wt %, the $CO_2$ permeability decreases slightly, whereas the corresponding $CO_2/H_2$ selectivity is only marginally affected (ranging from 2.1 to 2.5 in Figure 4b). At higher $PEG_{400}$ concentrations (>37 wt %), however, $P_{CO_2}$ and $\alpha_{CO_2/H_2}$ both increase dramatically (by ~160% and 87%, respectively, at 45 wt % $PEG_{400}$ relative to the neat SEOS copolymer) due most likely to a morphological transition to a continuous polyether microphase. Note that a blend with 37 wt % $PEG_{400}$ corresponds to about 65 wt % polyether, which would be a reasonable composition to expect a cylindrical morphology composed of S cylinders in an EO matrix. These pronounced increases in $CO_2$ permeability and selectivity due to the addition of $PEG_{400}$ testify to the high $CO_2$ solubility afforded by amorphous PEG solubilized within the SEOS nanostructure. The difference in gas-transport properties between $PEG_{400}$ and $PEG_{4600}$ is directly attributable to their disparate crystallinities, as discussed in the following section.

**Thermal Characteristics of SEOS/PEG Blends.** To ascertain whether the copolymer/homopolymer blend strategy depicted in Figure 1 is accurate, optical images of the neat SEOS copolymer and blends with $PEG_{4600}$ and $PEG_{400}$ at a concentration of 45 wt % PEG have been collected under crossed polars at ambient temperature. These images are displayed in Figure 5 and confirm that the neat copolymer is semicrystalline due to its high degree of birefringence (Figure 5a). Regions of strong birefringence increase substantially upon addition of $PEG_{4600}$ to the copolymer (Figure 5b). [The inset included in Figure 5b is obtained from the neat $PEG_{4600}$ homopolymer.] In marked contrast, the SEOS/PEG blend composed of $PEG_{400}$ (Figure 5c) exhibits very little birefringence, indicating that the polyether constituents of this blend are, for the most part, amorphous. Corresponding DSC thermograms acquired from the neat SEOS copolymer and the two blends pictured in Figure 5 are presented in Figure 6. Addition of $PEG_{4600}$ to the SEOS copolymer yields both a shift in normal melting temperature ($T_m$) to higher temperature and a concurrent increase in $\Delta H_m$, signifying a higher degree of crystallinity relative to the neat copolymer. In the case of $PEG_{400}$, however, the primary melting peak is shifted to a lower temperature and $\Delta H_m$ is reduced considerably. Included in the inset of Figure 6 is an enlargement of the thermogram collected from the neat SEOS copolymer showing the existence of the S glass transition temperature ($T_{g,S}$). Values of $T_m$ and $T_{g,S}$ gleaned from DSC thermograms of the neat copolymer and several SEOS/PEG blends such as those displayed in Figure 6 are provided as a function of PEG concen-

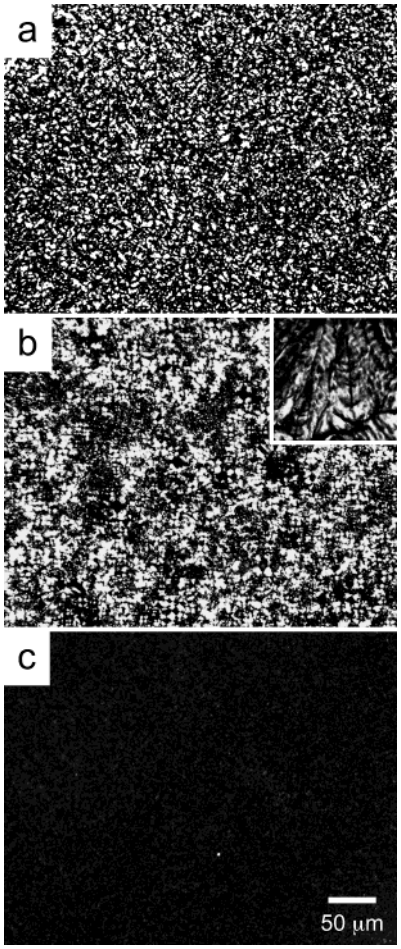


**Figure 5.** Polarized light micrographs of (a) the neat SEOS triblock copolymer, (b) a 55/45 SEOS/$PEG_{4600}$ blend, and (c) a 55/45 SEOS/$PEG_{400}$ blend at 23 °C. The inset in (b) shows the semicrystalline $PEG_{4600}$ homopolymer under crossed polars at the same magnification.

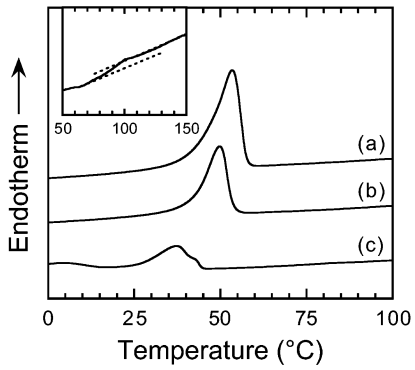


**Figure 6.** DSC thermograms acquired during the second heating cycle from (a) a 55/45 SEOS/$PEG_{4600}$ blend, (b) the neat SEOS triblock copolymer, and (c) a 55/45 SEOS/$PEG_{400}$ blend at a heating rate of 20 °C/min. The inset shows the upper (S) glass transition of the SEOS copolymer.

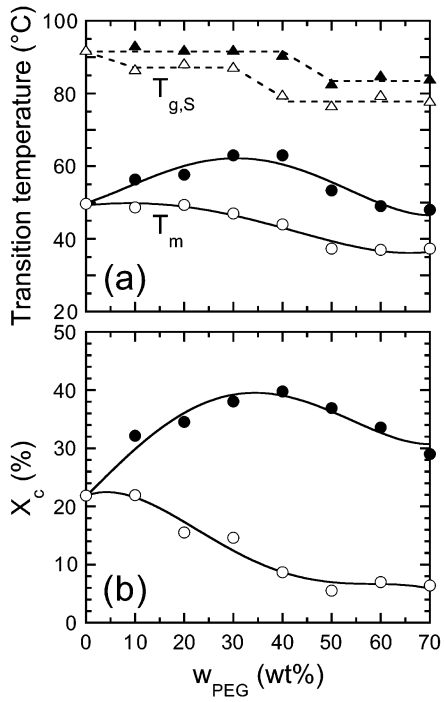


**Figure 7.** Dependence of (a) the EO normal melting temperature ($T_m$, circles) and S glass transition temperature ($T_{g,S}$, triangles) and (b) crystallinity ($X_c$) on blend composition in SEOS/PEG blends containing $PEG_{400}$ (open symbols) and $PEG_{4600}$ (filled symbols). The solid and dashed lines serve as guides for the eye.

tration for $PEG_{400}$ and $PEG_{4600}$ in Figure 7a, whereas corresponding crystallinities ($X_c$) computed from values of $\Delta H_m$ in conjunction with eq 2 are shown in Figure 7b.

Since the S block of the copolymer and PEG homopolymer are strongly incompatible and therefore remain largely unmixed, it is not surprising that $T_{g,S}$ is virtually independent of PEG addition up to ca. 40 wt % $PEG_{4600}$ in Figure 7a. The sharp drop in $T_{g,S}$ (by ~10 °C) in the vicinity of 50 wt % $PEG_{4600}$ suggests that the copolymer undergoes a $PEG_{4600}$-induced transition to a morphology that precludes the same degree of chain packing available to the S blocks in an alternating lamellar arrangement. A highly defective layered morphology or a dispersed morphology composed of S cylinders or spheres in an polyether-continuous matrix would be consistent with such a confinement effect. In the case of the lower molecular weight PEG, a reduction of ~5 °C is achieved with only 10 wt % $PEG_{400}$, thereby indicating limited incorporation of $PEG_{400}$ into the S lamellae. A further decrease in $T_{g,S}$ (of ~8 °C) similar to the one observed via addition of $PEG_{4600}$ also occurs in the SEOS/$PEG_{400}$ blend series, but at a lower PEG concentration (30−40 wt % for $PEG_{400}$, in contrast to 40−50 wt % $PEG_{4600}$). This shift in transition concentration is consistent with prior reports[4−7] of solvent- and homopolymer-induced morphological (order−order) transitions in block copolymer blends and reflects the ability of $PEG_{400}$ to more uniformly distribute within the EO microphases and consequently promote an increase in interfacial chain packing and an accompanying change in interfacial curvature at a lower concentration relative to $PEG_{4600}$. Values of $T_m$ shown in Figure 7a likewise display a difference for blends prepared with $PEG_{4600}$ and $PEG_{400}$. Upon addition of $PEG_{4600}$ ($T_m = 60$ °C), $T_m$ of the resultant SEOS/PEG copolymer blends (initially at 50 °C for the neat copolymer) increases up to 63 °C at 40 wt % $PEG_{4600}$ and then decreases to 48 °C at 70 wt %. This same trend is echoed in terms of $X_c$ for the SEOS/$PEG_{4600}$ blends in Figure 7b, suggesting that $PEG_{4600}$ not only swells the EO lamellae but also serves as a nucleating agent for the EO copolymer blocks. Concurrent reductions in $T_{g,S}$, $T_m$, and $X_c$ at ca. 50 wt % $PEG_{4600}$ in this SEOS/PEG blend series further support the existence of an order−order transition in the vicinity of this blend composition. The thermal signatures of the SEOS/$PEG_{400}$ blends in Figure 7, on the other hand, indicate that (i) $T_m$ and $X_c$ generally decrease with increasing $PEG_{400}$ content up to about 50 wt % and (ii) these reductions are relatively gradual. At $PEG_{400}$ concentrations greater than 50 wt %, both $T_m$ and $X_c$ become independent of blend composition.

The variation in $X_c$ promoted by the incorporation of either $PEG_{4600}$ or $PEG_{400}$ is expected to have a profound effect on the gas-transport properties of the resultant SEOS/PEG blends. Crystallites generally behave as impermeable obstacles that force penetrant molecules to diffuse through irregular, molecularly constricted conduits within accessible intercrystalline regions. The segmental mobility of the chains in the neighborhood of discrete crystallites is also affected, resulting in lower gas diffusivity, since these chains are covalently connected to the chains comprising the crystallites. Both factors decrease the penetrant diffusivity according to[51]

$$D = D_a/\tau\beta \tag{8}$$

where $D_a$ represents the diffusion coefficient of a penetrant molecule through a completely amorphous phase, $\tau$ is a tortuosity factor, and $\beta$ is the chain immobilization factor. Another way to describe the diffusion coefficient is as[38]

$$D = D_a\phi_a^{\,m} \tag{9}$$

where $\phi_a$ denotes the volume fraction of the amorphous phase, and $m$ (in the same fashion as $\tau$) provides an empirical measure of the effective diffusive path length (an increase in the value of $m$ signifies greater tortuosity). Since a diffusing penetrant species is virtually insoluble within crystalline regions, crystallites likewise hinder penetrant solubility, in which case the solubility can be expressed in analogous fashion as eq 9:

$$S = S_a\phi_a \tag{10}$$

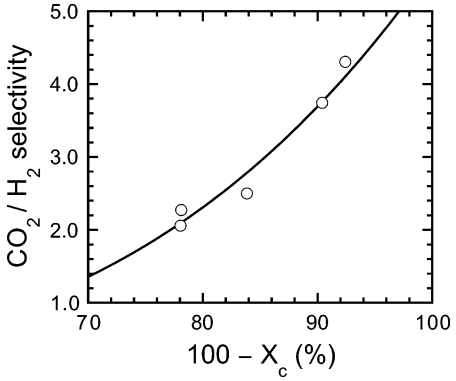


**Figure 8.** $CO_2/H_2$ selectivity at 35 °C as a function of the amorphous percentage ($100 - X_c$) for SEOS/$PEG_{400}$ blends varying in PEG concentration. The solid line is a linear regression of eq 12 to the data.

where $S_a$ is the solubility of a species in a purely amorphous polymer. Substitution of eqs 9 and 10 into eq 4 yields the permeability of a penetrant through a semicrystalline homopolymer, viz.

$$P = P_a \phi_a^{m+1} \tag{11}$$

Although the exponent $m$ can be calculated directly from measured values of $P$ and calculated values of $\phi_a$ (via $X_c$), its physical meaning is obscured due to the biphasic nature of the SEOS nanostructure. Generally speaking, the effective reduction in diffusivity arising from restricted molecular motion of polymer chains in the neighborhood of crystallites tends to increase with increasing penetrant size and is therefore expected to be more pronounced for $CO_2$ relative to $H_2$.[38] In this case, $m$ for $CO_2$ is expected to be larger than that for $H_2$ under identical conditions of crystal-induced tortuosity. A relative value of $\Delta m$ ($= m_{CO_2} - m_{H_2}$) can be computed from the $CO_2/H_2$ selectivity according to

$$\alpha_{CO_2/H_2} = (\alpha_{CO_2/H_2})_a \phi_a^{\Delta m} \tag{12}$$

Here, $(\alpha_{CO_2/H_2})_a$ is the $CO_2/H_2$ selectivity of the completely amorphous material. Since the mass densities of glassy homopolystyrene and amorphous/crystalline EO are not far removed from unity, $\phi_a$ can be reasonably approximated by $100 - X_c$ (where $X_c$ is expressed as a percentage). Figure 8 shows the dependence of $\alpha_{CO_2/H_2}$ on $100 - X_c$ and reveals that the data are favorably represented by eq 12 with $\Delta m > 0$ (~4) and $(\alpha_{CO_2/H_2})_a = 6.0$. While the value of $\Delta m$ is in agreement with intuitive expectation, it must be recognized, however, that the regressed value of $(\alpha_{CO_2/H_2})_a$ is not physically meaningful, since it reflects gas transport through the amorphous S *and* EO microphases (the morphology and fraction of which depend on blend composition).

**Temperature Effect on Gas Transport.** The permeabilities of $CO_2$ and $H_2$ are presented on semilogarithmic coordinates as functions of reciprocal temperature for the semicrystalline SEOS copolymer and 55/45 w/w SEOS/$PEG_{4600}$ blend in parts a and b of Figure 9, respectively. The linearity of the data at high and low temperature confirms that gas transport through these membranes is temperature-activated and can therefore be described by eq 6. In both semicrystalline materials, the permeabilities at low temperature (below $T_m$) are lower, and exhibit a distinctly different temperature dependence, than those at high temperature

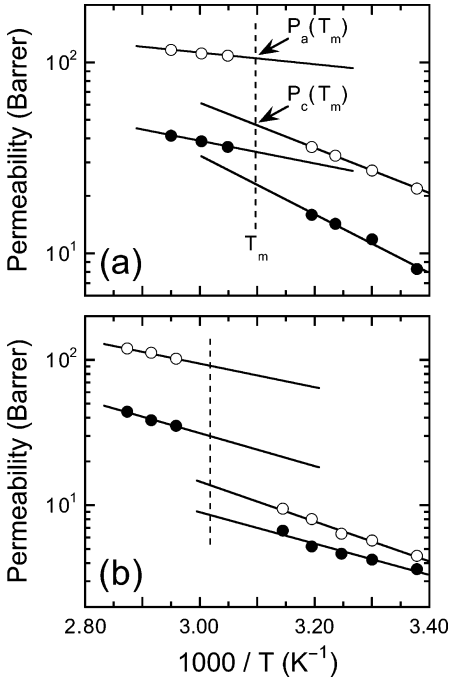


**Figure 9.** Variation of permeability with respect to reciprocal temperature for $CO_2$ (○) and $H_2$ (●) in (a) the neat SEOS triblock copolymer and (b) a 55/45 SEOS/$PEG_{4600}$ blend. The solid lines denote regressed fits of eq 6 to the data at low and high temperatures, whereas the dashed vertical lines identify the composition-dependent polyether melting temperature obtained from Figure 7a. The positions of $P_a(T_m)$ and $P_c(T_m)$ for $CO_2$ are labeled for illustrative purposes in (a).

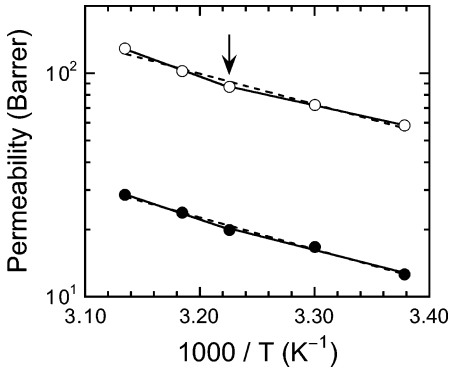


**Figure 10.** Permeability as a function of reciprocal temperature for $CO_2$ (○) and $H_2$ (●) in a 55/45 SEOS/$PEG_{400}$ blend. The solid lines are regressed fits of eq 6 to the data at low and high temperatures, the dashed line is a single regression to all the data, and the arrow identifies $T_m$.

(above $T_m$, but below $T_{g,S}$). Comparison of results obtained from the analogous 55/45 SEOS/$PEG_{400}$ blend (see Figure 10), which does not exhibit such variation, indicates that the change in permeability temperature dependence observed in Figure 9 can be unambiguously attributed to the existence of crystals within the polyether microphase. It is important to note that, in all these variable-temperature permeation measurements (which traverse $T_m$ of the polyether), a microphase-ordered nanostructure remains intact to provide the SEOS/PEG blends with sufficient mechanical integrity. Thus, we extend the previous studies of Hirayama et al.[21] and Okamoto et al.[23] by discerning the effect of polyether melting on gas-transport properties as a function of composition in blends of the SEOS copolymer with $PEG_{4600}$. This analysis cannot be conducted for the

**Table 3. Apparent Activation Energies for $CO_2$ and $H_2$ Permeation in the SEOS Copolymer and Its Blends with PEG[a]**

| | | $E_{P,c}$ (kJ/mol) | | $E_{P,a}$ (kJ/mol) | | $\Delta E_{P,m}$ (kJ/mol) | |
|---|---|---|---|---|---|---|---|
| membrane | $w_{PEG}$ (wt %) | $CO_2$ | $H_2$ | $CO_2$ | $H_2$ | $CO_2$ | $H_2$ |
| SEOS | 0 | 22.8 | 29.5 | 5.97 | 11.3 | −16.8 | −18.2 |
| SEOS + $PEG_{4600}$ | 10 | 48.3 | 51.1 | 12.4 | 22.8 | −35.9 | −28.3 |
| | 30 | 51.4 | 31.0 | 1.84 | 6.09 | −49.6 | −24.9 |
| | 45 | 26.5 | 20.4 | 15.9 | 21.8 | −10.6 | +1.38 |
| SEOS + $PEG_{400}$ | 45 | 21.7 | 24.9 | 21.7 | 24.9 | | |

[a] Values are extracted from data such as those presented in Figure 9 in conjunction with eq 6.

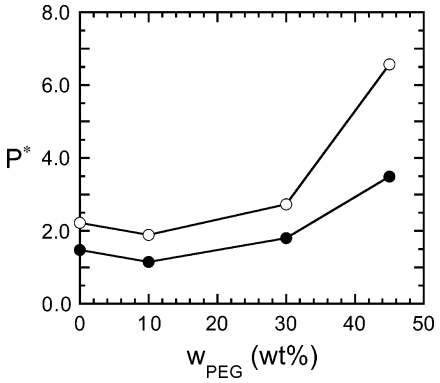


**Figure 11.** Dependence of the permeability switch ($P^*$) on blend composition for $CO_2$ (○) and $H_2$ (●) in SEOS/$PEG_{4600}$ blends. The solid lines connect the data.

SEOS/$PEG_{400}$ blends due to their apparently low crystallinity (see Figure 7b).

One way to characterize the change in permeability upon melting is through a permeability switch ($P^*$), which is defined as

$$P^* = P_a(T_m)/P_c(T_m) \tag{13}$$

Here, $P_c$ is the permeability of the semicrystalline membrane. Since the permeability cannot be measured at $T_m$, values of $P_a(T_m)$ and $P_c(T_m)$ are computed by using eq 6 to extrapolate the temperature-dependent $P_a$ and $P_c$ to $T_m$ evaluated from Figure 7a, in which case

$$P^* = (P_{0a}/P_{0c}) \exp(-\Delta E_{P,m}/RT_m) \tag{14}$$

where $P_{0a}$ and $P_{0c}$ are the frequency factors of the amorphous and semicrystalline membranes, and $\Delta E_{P,m}$ is the change in the apparent activation energy for permeation upon melting (= $E_{P,a} - E_{P,c}$, where the subscripted "a" and "c" have the same meaning as above). Values of $E_{P,a}$, $E_{P,c}$, and $\Delta E_{P,m}$ determined for $CO_2$ and $H_2$ in the SEOS copolymer and three SEOS/$PEG_{4600}$ blends are provided in Table 3. The dependence of $P^*$ on $PEG_{4600}$ content is displayed in Figure 11, which reveals that $P^*$ is (i) consistently larger for $CO_2$ relative to $H_2$ and (ii) weakly dependent on $w_{PEG}$ up to 30 wt % $PEG_{4600}$. Increasing the $PEG_{4600}$ concentration to 45 wt %, however, promotes a sharp increase in $P^*$ for $CO_2$, as well as a less pronounced increase in $P^*$ for $H_2$, which is again consistent with a morphological transition to a polyether-continuous nanostructure in the vicinity of 40 wt % $PEG_{4600}$ (see Figure 7a).

It is interesting that $\Delta E_{P,m}$ for $CO_2$ tends to decrease substantially (from −16.8 to −49.6 kJ/mol), while that for $H_2$ exhibits less composition dependence, with increasing $PEG_{4600}$ concentration up to 30 wt %. Following the same trend displayed by $P^*(w_{PEG})$ in Figure 11, $\Delta E_{P,m}$ for both $CO_2$ and $H_2$ likewise shows a dramatic increase at 45 wt % $PEG_{4600}$. Since $E_P$ constitutes the summation of activation energies arising from diffusion ($E_D$) and sorption ($E_S$),[52] we can qualitatively describe how these contributions differ for $CO_2$ and $H_2$. Since $H_2$ is physically smaller than $CO_2$, $E_D$ is generally expected (and has been shown[53]) to be smaller for $H_2$ relative to $CO_2$. Conversely, since $CO_2$ is more condensable in and can interact specifically with the polar linkages of the polyether microphase, it should have a smaller $E_S$ compared to that of $H_2$. Combining these contributions yields comparable magnitudes of $E_P$ for both $CO_2$ and $H_2$, which, for the most part, are observed for the semicrystalline SEOS copolymer and its blends with $PEG_{4600}$ at temperatures below $T_m$ (see Table 3). Only the blend with 30 wt % $PEG_{4600}$ deviates substantially (and reproducibly) from this expectation and warrants further investigation. Comparison of the results listed in Table 3 reveals that $E_P$ is generally in excess of 20 kJ/mol. At temperatures above $T_m$, however, the values of $E_P$ for $CO_2$ and $H_2$ are observed to differ significantly, indicating that another aspect of $E_P$ must be considered. Under these conditions, $E_P$ for $CO_2$ and $H_2$ permeation through the glassy S microphase is of the same magnitude as that for $CO_2$ and $H_2$ through the amorphous EO microphase (see Table 1), confirming that this contribution to the overall gas-transport process cannot be neglected. Over the temperature range illustrated in Figure 9, the changes in permeability of $CO_2$ and $H_2$ through polystyrene, calculated from the frequency factors and activation energies provided in Table 1, are 7.8 and 31 Barrers, respectively.

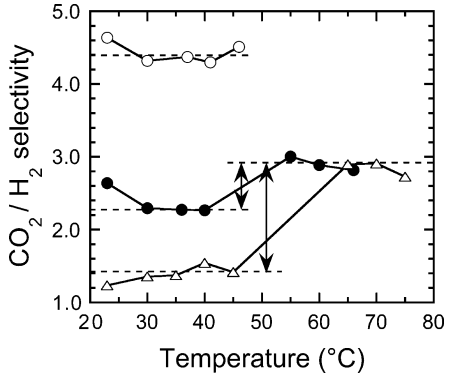


**Figure 12.** $CO_2/H_2$ selectivity as a function of temperature for the neat SEOS copolymer (●), a 55/45 SEOS/$PEG_{400}$ blend (○), and a 55/45 SEOS/$PEG_{4600}$ blend (△). The solid lines connect the data, and the dashed horizontal lines represent guides to show relevant trends. The arrows identify the change in $CO_2/H_2$ selectivity upon polyether melting.

With this apparent limitation of the present membranes notwithstanding, the $CO_2/H_2$ selectivities of the neat SEOS copolymer and the 55/45 SEOS/PEG blends with $PEG_{4600}$ and $PEG_{400}$ are presented as a function of temperature in Figure 12 and confirm that $\alpha_{CO_2/H_2}$ for the SEOS/$PEG_{400}$ blend remains relatively constant across its polyether melting transition. In this case, the reduction in solubility selectivity promoted by an increase in temperature is offset by enhanced $CO_2$ diffusivity (relative to $H_2$ diffusivity) so that the overall $CO_2/H_2$ selectivity shows very little dependence on temperature. Both semicrystalline membranes, however, undergo an abrupt increase in $\alpha_{CO_2/H_2}$ upon melting, with the

magnitude of this change in selectivity increasing with increasing blend crystallinity. The melting of EO crystals in the neat SEOS copolymer and the SEOS/$PEG_{4600}$ blend promotes a reduction in diffusion selectivity, but an increase in $CO_2$ solubility selectivity, which we contend dominates the net selectivity due to the increased availability of ether linkages accessible for interaction with diffusing $CO_2$ molecules.

## Conclusions

The gas-permeation properties of $CO_2$, $H_2$, $N_2$, and $O_2$ have been measured as a function of composition in a microphase-ordered (lamellar) SEOS triblock copolymer with a polyether midblock as well as in its miscible blends with PEG differing in molecular weight. If the added PEG is semicrystalline, blends with the SEOS copolymer are observed to exhibit elevated melting temperatures and enhanced crystallinity due to nucleation of the EO blocks residing within the confined polyether lamellae. Incorporation of amorphous PEG into the SEOS copolymer results in reduced S glass transition and EO melting temperatures, as well as a decrease in the overall crystallinity. All the membranes consistently exhibit higher $CO_2$ permeability than $H_2$ due to the unusually high solubility of $CO_2$ in the polyether, thereby confirming that the polyether microphase constitutes the main locus of gas transport within these biphasic materials at temperatures below the polyether melting temperature. Under these conditions, the presence of EO crystals lowers $CO_2/H_2$ selectivity because crystalline regions serve as impermeable obstacles to molecular diffusion and likewise reduce solubility due to inaccessibility of the polymer chains. In this regard, an increase in blend crystallinity (as in the case of the SEOS/$PEG_{4600}$ blends) promotes an overall reduction in $CO_2/H_2$ selectivity. At sufficiently high PEG concentrations, the gas-transport and thermal properties indicate the existence of a morphological transition to a polyether-continuous nanostructure. Details of this transition and of the corresponding morphologies in PEG- and S-rich SEOS/PEG blends are forthcoming.[39] Abrupt increases in $CO_2$ and $H_2$ permeability are observed upon heating the neat SEOS copolymer and the SEOS/$PEG_{4600}$ blends due to polyether crystal melting within copolymer-stabilized nanostructured membranes. A permeation switch determined at the composition-dependent melting point and the temperature-dependent $CO_2/H_2$ selectivity together reveal that $CO_2$ permeation is more strongly influenced than $H_2$ permeation by such crystal melting, especially in light of an apparent morphological transition at relatively high $PEG_{4600}$ concentrations. The results reported herein confirm that microphase-ordered block copolymers containing a polyether block can serve as reverse-selective membranes exhibiting high $CO_2$ specificity. We have shown that, through judicious choice of PEG molecular weight and blend composition, the gas-transport and thermal properties of near-equilibrium SEOS/PEG blends can be systematically tailored using the design paradigms[4] established for block copolymer/homopolymer (or solvent) blends.

**Acknowledgment.** This work was supported by the U.S. Department of Energy under Contract DE-FG02-99ER14991.

## References and Notes

(1) Bates, F. S.; Fredrickson, G. H. *Phys. Today* **1999**, *52*, 32.
(2) Hamley, I. W. *The Physics of Block Copolymers*; Oxford University Press: Oxford, 1998.
(3) Hadjichristidis, N.; Pispas, S.; Floudas, G. A *Block Copolymers: Synthetic Strategies, Physical Properties, and Applications*; Wiley-Interscience: New York, 2003.
(4) Spontak, R. J.; Patel, N. P. In *Developments in Block Copolymer Science and Technology*; Hamley, I. W., Ed.; Wiley: New York, 2004; pp 159−212.
(5) Hanley, K. J.; Lodge, T. P. *J. Polym. Sci., Part B: Polym. Phys.* **1998**, *36*, 3101. Lodge, T. P.; Pudil, B.; Hanley, K. J. *Macromolecules* **2002**, *35*, 4707.
(6) Laurer, J. H.; Khan, S. A.; Spontak, R. J.; Satkowski, M. M.; Grothaus, J. T.; Smith, S. D.; Lin, J. S. *Langmuir* **1999**, *15*, 7947.
(7) Winey, K. I.; Thomas, E. L.; Fetters, L. J. *J. Chem. Phys.* **1991**, *95*, 9367. Winey, K. I.; Thomas, E. L.; Fetters, L. J. *Macromolecules* **1991**, *24*, 6182; **1992**, *25*, 2645. Urbas, A.; Sharp, R.; Fink, Y.; Thomas, E. L.; Xenidou, M.; Fetters, L. J. *Adv. Mater.* **2000**, *12*, 812.
(8) Tanaka, H.; Hashimoto, T. *Macromolecules* **1991**, *24*, 5713. Kimishima, K.; Hashimoto, T.; Han, C. D. *Macromolecules* **1995**, *28*, 3842. Bodycomb, J.; Yamaguchi, D.; Hashimoto, T. *Macromolecules* **2000**, *33*, 5187.
(9) Schulz, M. F.; Bates, F. S.; Almdal, K.; Mortensen, K. *Phys. Rev. Lett.* **1994**, *73*, 86. Zhao, J.; Majumdar, B.; Schulz, M. F.; Bates, F. S.; Almdal, K.; Mortensen, K.; Hajduk, D. A.; Gruner, S. M. *Macromolecules* **1996**, *29*, 1204.
(10) Kane, L.; Satkowski, M. M.; Smith, S. D.; Spontak, R. J. *Macromolecules* **1996**, *29*, 8862. Spontak, R. J.; Fung, J. C.; Braunfeld, M. B.; Sedat, J. W.; Agard, D. A.; Kane, L.; Smith, S. D.; Satkowski, M. M.; Ashraf, A.; Hajduk, D. A.; Gruner, S. M. *Macromolecules* **1996**, *29*, 4494. Kane, L.; Norman, D. A.; White, S. A.; Matsen, M. W.; Satkowski, M. M.; Smith, S. D.; Spontak, R. J. *Macromol. Rapid Commun.* **2001**, *22*, 281.
(11) Abetz, V.; Goldacker, T. *Macromol. Rapid Commun.* **2000**, *21*, 16.
(12) Yamaguchi, D.; Shiratake, S.; Hashimoto, T. *Macromolecules* **2000**, *33*, 8258. Yamaguchi, D.; Hashimoto, T. *Macromolecules* **2001**, *34*, 6495. Yamaguchi, D.; Hasegawa, H.; Hashimoto, T. *Macromolecules* **2001**, *34*, 6506. Yamaguchi, D.; Takenaka, M.; Hasegawa, H.; Hashimoto, T. *Macromolecules* **2001**, *34*, 1707. Court, F.; Hashimoto, T. *Macromolecules* **2001**, *34*, 2536. Court, F.; Hashimoto, T. *Macromolecules* **2002**, *35*, 2566.
(13) Park, C.; Yoon, J.; Thomas, E. L. *Polymer* **2003**, *44*, 6725.
(14) Bronstein, L. M. *Top. Curr. Chem.* **2003**, *226*, 55.
(15) Simon, P. F. W.; Ulrich, R.; Spiess, H. W.; Wiesner, U. *Chem. Mater.* **2001**, *13*, 3464.
(16) Jonquières, A.; Clément, R.; Lochon, P. *Prog. Polym. Sci.* **2002**, *27*, 1803 and references provided therein.
(17) Stern, S. A. *J. Membr. Sci.* **1994**, *94*, 1. Ghosal, K.; Freeman, B. D. *Polym. Adv. Technol.* **1994**, *5*, 673.
(18) Bhide, B. D. Stern, S. A. *J. Membr. Sci.* **1993**, *81*, 209; **1993**, *93*, 239.
(19) Merkel, T. C.; He, Z. J.; Pinnau, I.; Freeman, B. D.; Meakin, P.; Hill, A. J. *Macromolecules* **2003**, *36*, 8406. Merkel, T. C.; Freeman, B. D.; Spontak, R. J.; He, Z.; Pinnau, I.; Meakin, P.; Hill, A. J. *Chem. Mater.* **2003**, *15*, 109. Merkel, T. C.; Freeman, B. D.; Spontak, R. J.; He, Z.; Pinnau, I.; Meakin, P.; Hill, A. J. *Science* **2002**, *296*, 519.
(20) Saha, S.; Chakma, A. *Energy Convers. Manage.* **1992**, *33*, 413. Davis, R. A.; Sandall, O. C. *AIChE J.* **1993**, *39*, 1135.
(21) Hirayama, Y.; Kase, Y.; Tanihara, N.; Sumiyama, Y.; Kusuki, Y.; Haraya, K. *J. Membr. Sci.* **1999**, *160*, 87.
(22) Patel, N. P.; Miller, A. C.; Spontak, R. J. *Adv. Mater.* **2003**, *15*, 729. Patel, N. P.; Miller, A. C.; Spontak, R. J. *Adv. Funct. Mater.*, in press.
(23) Okamoto, K.-I.; Fujii, M.; Okamyo, S.; Suzuki, H.; Tanaka, K.; Kita, H. *Macromolecules* **1995**, *28*, 6950.
(24) Bondar, V. I.; Freeman, B. D.; Pinnau, I. *J. Polym. Sci., Part B: Polym. Phys.* **1999**, *37*, 2463; **2000**, *38*, 2051.
(25) Kim, J. H.; Seong, Y. H.; Lee, Y. M. *J. Membr. Sci.* **2001**, *190*, 179.
(26) Spontak, R. J.; Smith, S. D. *J. Polym. Sci., Part B: Polym. Phys.* **2001**, *39*, 947.
(27) Kinning, D. J.; Thomas, E. L.; Ottino, J. M. *Macromolecules* **1987**, *20*, 1129.
(28) Csernica, J.; Baddour, R. F.; Cohen, R. E. *Macromolecules* **1987**, *20*, 2468; **1989**, *22*, 1493. Rein, D. H.; Csernica, J.; Baddour, R. F.; Cohen, R. E. *Macromolecules* **1990**, *23*, 4456. Csernica, J.; Rein, D. H.; Baddour, R. F.; Cohen, R. E. *Macromolecules* **1991**, *24*, 3612. Rein, D. H.; Baddour, R. F.; Cohen, R. E. *J. Appl. Polym. Sci.* **1992**, *45*, 1223.

(29) Zielinski, J. M. In *Encyclopedia of Materials: Science and Technology*; Buschow, K. H. J., Cahn, R. W., Flemings, M. C., Ilschner, B., Kramer, E. J., Mahajan, S., Eds.; Elsevier: Amsterdam, 2001; Vol. 1.
(30) Sax, J.; Ottino, J. M. *Polym. Eng. Sci.* **1983**, *23*, 165. Sax, J.; Ottino, J. M. *Polymer* **1985**, *26*, 1073.
(31) Faridi, N.; Duda, J. L.; Hadj Romdhane, I. *Ind. Eng. Chem. Res.* **1995**, *34*, 3556.
(32) Vrentas, J. S.; Vrentas, C. M. *Chem. Eng. Sci.* **1997**, *52*, 985.
(33) Arnold, M. E.; Nagai, K.; Freeman, B. D.; Spontak, R. J.; Leroux, D.; Betts, D. E.; DeSimone, J. M.; DiGiano, F. A.; Stebbins, C. K.; Linton, R. W. *Macromolecules* **2002**, *35*, 3697. Arnold, M. E.; Nagai, K.; Freeman, B. D.; Spontak, R. J.; Betts, D. E.; DeSimone, J. M.; Pinnau, I. *Macromolecules* **2001**, *34*, 5611.
(34) Felder, R. M.; Huvard, G. S. *Permeation, Diffusion and Sorption of Gases and Vapors*; Fava, R., Ed.; Academic Press: New York, 1978; Vol. 16C, p 315.
(35) Geng, H. Z.; Rosen, R.; Zheng, B.; Shimoda, H.; Fleming, L.; Liu, J.; Zhou, O. *Adv. Mater.* **2002**, *14*, 1387.
(36) Wijmans, J. G.; Baker, R. W. *J. Membr. Sci.* **1995**, *107*, 1.
(37) Freeman, B. D.; Pinnau, I. *Trends Polym. Sci.* **1997**, *5*, 167.
(38) Weinkauf, D. H.; Paul, D. R. In *Barrier Polymers and Barrier Structures*; Koros, W. J., Ed.; American Chemical Society: Washington, DC, 1990; pp 60−91. Petropoulos, J. H. In *Polymeric Gas Separation Membranes*; Paul, D. R., Yampol'skii, Y. P., Eds.; CRC Press: Boca Raton, FL, 1994; p 17.
(39) Patel, N. P.; Spontak, R. J. Manuscript in preparation.
(40) Patel, N. P.; Spontak, R. J. *Macromolecules* **2004**, *37*, 1394.
(41) Merkel, T. C.; Bondar, V. I.; Nagai, K.; Freeman, B. D.; Pinnau, I. *J. Polym. Sci., Part B: Polym. Phys.* **2000**, *38*, 415.
(42) Zolandz, R. R.; Fleming, G. K. In *Membrane Handbook*; Ho, W. S. W., Sirkar, K. K., Eds.; Van Nostrand Reinhold: New York, 1992; pp 17−101.
(43) Yamada, S.; Nakagawa, T. *Kobunshi Ronbunshu* **1982**, *39*, 391.
(44) Robeson, L. M.; Noshay, A.; Matzner, M.; Merriam, C. N. *Angew. Makromol. Chem.* **1973**, *29/30*, 47.
(45) Maxwell, C. *Treatise on Electricity and Magnetism*; Oxford University Press: London, 1873; Vol. 1.
(46) Subramanian, P. M.; Plotzker, I. G. In *Polymer Blends*; Paul, D. R., Bucknall, C. B., Eds.; Wiley: New York, 2000; Vol. 2, Chapter 30.
(47) Michaels, A. S.; Bixler, H. J. *J. Polym. Sci.* **1961**, *50*, 413.
(48) Amerongen, G. J. V. *Rubber Chem. Technol.* **1964**, *37*, 1065.
(49) Reid, R. C.; Prausnitz, J. M.; Poling, B. E. *The Properties of Gases and Liquids*; McGraw-Hill: New York, 1987; p 741.
(50) Breck, D. W. *Zeolite Molecular Sieves*; Wiley-Interscience: New York, 1974; p 65.
(51) Michaels, A. S.; Bixler, H. J. *J. Polym. Sci.* **1961**, *50*, 393.
(52) Kim, J. H.; Seong, Y. H.; Lee, Y. M. *J. Membr. Sci.* **2001**, *193*, 209.
(53) Petropoulos, J. H. *J. Membr. Sci.* **1990**, *53*, 229.

MA049975K